CORROSION SCIENCE AND TECHNOLOGY, Vol.25, No.4(2026), pp.232~246 pISSN 1598-6462 / eISSN 2288-6524
[Research Paper] DOI: https://doi.org/10.14773/cst.2026.25.4.232

Hydrodynamic Threshold Governing $FeCO_3$ Film Breakdown in CO_2 Corrosion of X65 Carbon Steel

Khalid Abdulhussain Mohammed[1,†] and Mustafa Hashim[2]

[1]*Oil and Gas Department, College of Engineering, University of Thi-Qar, Thi-Qar, Iraq*
[2] *Add Value Consultancy Ltd, Aberdeen, UK*

(Received March 05, 2026; Revised June 30, 2026; Accepted June 30, 2026)

The formation of protective iron carbonate ($FeCO_3$) films is crucial for mitigating corrosion in carbon steel pipelines operating in CO_2-containing environments. However, accurately quantifying the long-term stability of these films under realistic hydrodynamic conditions remains a challenge. This study investigates the hydrodynamic conditions that govern the chemical dissolution of $FeCO_3$ films formed on X65 carbon steel in CO_2-saturated brine.Using a controlled, stepped-flow experimental technique, pre-existing protective films were exposed to progressively increasing shear conditions while maintaining constant chemistry. Weight-loss measurements, surface characterization, and film morphology analysis revealed a hydrodynamic threshold. Beyond this threshold, protective films rapidly degrade, and corrosion rates sharply increase. The findings demonstrate a critical operating envelope that separates protective and non-protective regimes. This transition is driven by flow-enhanced chemical undersaturation at the steel interface, rather than mechanical detachment. By defining threshold values for solution pH and wall shear stress that govern $FeCO_3$ film stability, this study provides new mechanistic insight into the coupled chemical–hydrodynamic processes controlling protective film removal during CO_2 corrosion of carbon steel pipelines.

Keywords: *Wall shear stress, Scale removal, Film stability, Flow-induced corrosion, Pipeline integrity*

1. Introduction

The transportation of unprocessed oil and gas through carbon-steel pipelines is a critical stage in oil and gas production. When the process fluid leaves the oil well, it is generally unprocessed and comprises multiple phases of oil, solids, gas, and brine. The presence of brine in conjunction with various dissolved acidic gases such as carbon dioxide (CO_2) and hydrogen sulphide (H_2S), along with organic acids, can result in corrosion problems on the internal walls of carbon steel pipelines, manifesting themselves through several different mechanisms, some more serious and difficult to control than others [1,2]. A complex interplay of aqueous chemistry, gas composition, and hydrodynamic conditions governs the CO_2 corrosion rates. Understanding the mechanism of CO_2 corrosion and predicting the risk, developing improved corrosion mitigation techniques, and understanding how the formation and stability of protective $FeCO_3$ films are, therefore, crucial for developing effective corrosion management strategies [3,4].

The formation of protective corrosion product layers on carbon steel can result in reduced corrosion rates in CO_2-containing environments. In particular, iron carbonate ($FeCO_3$) films act as diffusion barriers that limit the transport of corrosive species to the metal surface. When $FeCO_3$ films are compact and well adhered, they can greatly suppress the corrosion rates; however, any deterioration, removal, or localized breakdown of these films can cause substantial metal loss and accelerated corrosion. Therefore, the stability of $FeCO_3$ films under operating conditions is a key factor in maintaining pipeline integrity [5-9].

Fluid flow significantly impacts $FeCO_3$ film formation and stability. The corrosion mechanism is influenced by modifying the turbulence near the pipe surface, altering mass transport conditions, and imposing hydrodynamic forces on corrosion product layers [10,11]. To characterize hydrodynamic severity, numerous studies have investigated the influence of flow on corrosion rates and protective

†Corresponding author: dr.khalid@utq.edu.iq

film stability, which often use parameters such as flow velocity or wall shear stress [12,13]. Wall shear stress, in particular, is frequently proposed as a key parameter governing mechanical film removal; however, reported critical stress values are generally much lower than those required to cause direct mechanical detachment of $FeCO_3$ films. This suggests that purely mechanical removal is unlikely to be the dominant degradation mechanism under single-phase aqueous flow conditions [13-16].

Consequently, many investigations suggest that the removal of $FeCO_3$ film in flowing systems is predominantly governed by chemical dissolution rather than mechanical erosion. Ruzić et al. [17] showed that mean and changing wall shear stresses alone cannot explain how mechanical forces can remove films, especially when the flow is turbulent and single-phase. Other studies have stressed the importance of turbulence near walls and localized flow disturbances, suggesting that hydrodynamic effects may indirectly reduce film adhesion rather than physically detach the film from the surface [13,18].

The solution pH and the iron carbonate saturation level significantly affect the chemical stability of $FeCO_3$ films. At low pH and under unsaturated conditions, the thermodynamic stability of the protective layer decreases [19,20].

Previous research [13,21,22] has confirmed that surface reaction kinetics and the dissolution behavior of iron carbonate ($FeCO_3$) primarily influence its dissolution, and that flow velocity has a negligible effect within the studied range. However, all previous intensive studies conducted under steady-state and low-flow conditions failed to establish a quantitative hydrodynamic threshold for film failure under chemical saturation experimentally, nor did they determine whether the failure of the iron carbonate ($FeCO_3$) film in single-phase flow is due to direct mechanical removal or to chemically driven dissolution enhanced by hydrodynamic mass transfer. Understanding this transfer is crucial for accurate pipeline corrosion prediction because it defines the critical limit at which hydrodynamic shear exceeds the film's chemical stability.

This study examines the impact of solution chemistry and flow conditions on the stability of protective $FeCO_3$ films on X65 carbon steel, utilizing a newly developed stepped shear recirculating flow loop. Flow velocity was recorded as an operational parameter, while wall shear stress served as the primary basis for comparison, as it better represents the near-surface hydrodynamic conditions influencing film integrity across various flow geometries.

Pre-formed iron carbonate films were evaluated under precisely controlled no-flow and flow conditions relevant to pipeline operation. This work was designed to define the pH threshold at which $FeCO_3$ films retain integrity at 50 ºC and to investigate how wall shear stress and flow velocity affect film stability at this critical condition. Special emphasis was placed on clarifying the relative contributions of mechanically induced film damage and hydrodynamically assisted chemical dissolution. The results delineate a transition threshold between stable and destabilized film behavior and provide measurable information useful for corrosion assessment in CO_2 transport pipelines.

2. Experimental procedure

The experiments in this study were conducted using a custom-designed flow loop (Fig. 1) and comprised three sequential stages:

· Formation of $FeCO_3$ films on X65 carbon steel at 60 ºC and 100 bar CO_2.

· Evaluation of film stability under static aqueous conditions at 50 ºC.

· Investigation of film degradation under controlled flowing conditions at 50 ºC.

After exposure, surface and cross-sectional characterization were carried out using scanning electron microscopy (SEM) and energy dispersive spectroscopy (EDS).

2.1 Material and Sample Preparation

All test coupons were machined from X65 carbon steel and prepared with a cylindrical shape measuring 10 mm in diameter and 25 mm in thickness. Prior to testing, the surface samples were sequentially polished with 600-grit silicon carbide paper, rinsed with distilled water, cleaned with isopropyl alcohol, and dried with warm air. To prevent galvanic interaction with the autoclave body, samples were mounted on polytetrafluoroethylene (PTFE) holders during all formation tests.

2.2 Formation of $FeCO_3$ Films

$FeCO_3$ films were formed using a high-pressure autoclave system at 100 bar CO_2 and 60 ºC. The setup

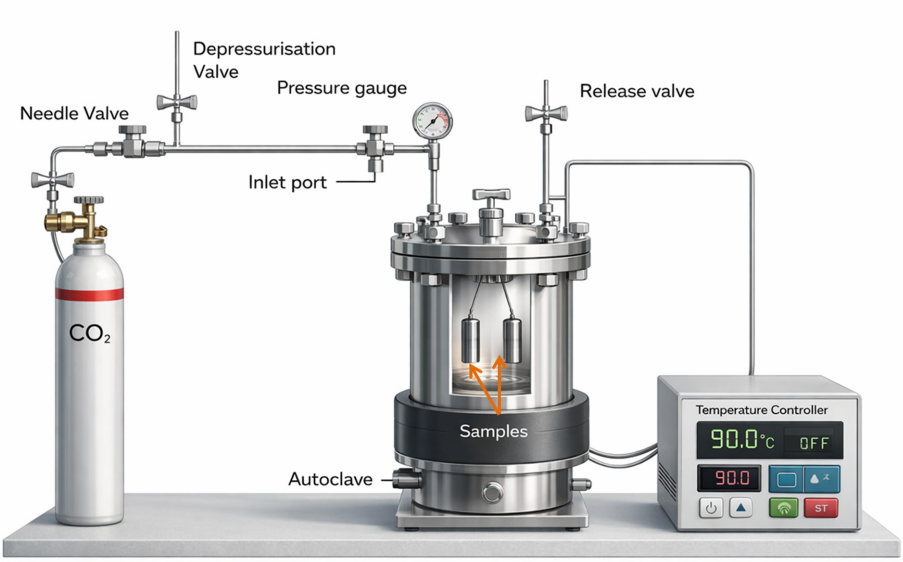

Fig. 1. Schematic diagram of the high-pressure CO_2 corrosion setup used for $FeCO_3$ film formation under controlled temperature and pressure conditions

consists of a 1-litre pressure vessel autoclave with high-pressure pipes and valves to control the CO_2 flowing, and temperature and pressure gauges to monitor the conditions throughout the test period continuously. Prior to the film forming, distilled water was purged with CO_2 gas in a separate container for at least 12 hours to ensure a CO_2-saturated solution and a fully deoxygenated system. To identify the critical immersion time at which the $FeCO_3$ films develop a dense and continuous structure fully covering the carbon steel surface and stable thickness, a series of five formation tests was conducted for different exposure durations (6, 24, 48, 96, and 192 h) under high-pressure CO_2 conditions, which was subsequently adopted as the standard immersion time for all subsequent formation experiments. The solution pH inside the autoclave was measured with a high-pressure pH probe, yielding values ranging from 3.25 to 3.45.

2.3 Weight Loss Measurements

After each formation test, X65 specimens were softly dried and weighed using an analytical balance with ±0.05 mg accuracy to determine mass gain. Corrosion products were then removed using the Clarke solution prepared according to ASTM G1-03 [23] Then, the specimens were rinsed with distilled water, followed by ethanol, and dried with the air gun.

Corrosion rates were calculated using the weight loss method according to the following equation:

$$CR = \frac{87.6 m_{loss}}{\rho_{Fe} A t}$$

where CR is the calculated corrosion (mm/y); m_{loss} is the mass loss of the sample (measured in grams); ρ_{Fe} is the density of iron (equal to 7.85 g/cm^3); A is the surface area (in cm^2), and t represents the exposure time (in hours).

2.4 Static Film Stability Tests

After the formation of $FeCO_3$ films, a series of static exposure tests was carried out to examine the stability and protective effectiveness of the films in aqueous environments. The objective of these tests was to identify the critical solution pH at which the iron carbonate layer remained intact, with no detectable film degradation at 50 ºC. Film stability was assessed at three pH values, as listed in Table 1, while all other experimental conditions were kept constant.

Static tests were performed in a conventional three-electrode glass cell. Before testing, $FeCO_3$-coated samples were mounted in a non-conductive resin, leaving only the film-covered surface exposed to the electrolyte. Care was taken during mounting to avoid mechanical damage or contamination of the protective iron carbonate layer. The

glass cell held 1 L of deionized water containing 3 wt% NaCl To reach CO_2 saturation and lower the amount of dissolved oxygen, the electrolyte was flushed with high-purity CO_2 (99.9%) at a rate of 50 mL/min for about 2 hours. CO_2 bubbling was maintained throughout the experiment to preserve the test environment. After which the electrolyte was heated to and maintained at 50 ºC throughout the test.

To determine instantaneous corrosion rates, a Gill ACMT 12 multi-channel potentiostat was used in a three-electrode configuration, with an AISI 1020 carbon steel working electrode (WE), a saturated Ag/AgCl reference electrode (RE), and a platinum counter electrode (CE). The linear polarization resistance (LPR) test starts at -15 mV of the open circuit potential (OCP) and ends at 15 mV, with a rate of 10 mV per minute.

The specimens were allowed to air dry and stored in a vacuum-deaerated jar to prevent oxidation and corrosion before surface analysis by scanning electron microscopy (SEM).

2.5 Flowing Condition Tests

A recirculating flow loop system was designed to investigate flow-induced degradation of $FeCO_3$ films. A schematic of the test setup and geometry is detailed in Fig. 2. The system has a stepped-shear flow cell with height and width varied along the flow path. This design enables those different wall shear stresses to be applied to several specimens in a single test.

Flow rates were induced using a Calpeda MX HL405/B multistage centrifugal pump equipped with a variable-speed drive and continuously monitored using an IFM SU7000 flow meter. Although both flow velocity and wall shear stress were determined, the latter was used for evaluation because it is more directly linked to near-wall transport and film degradation. By changing channel shapes and controlled flow rates, the resulting wall shear stresses reached about 10 to 655 Pa, which corresponded to flow speeds of 1.5 to 13.9 m/s.

The electrolyte was prepared from deionized water

Table 1. Static conditions test matrix.

Condition	Solution	Temperature	pH	Exposure time	Purpose
1	CO_2-saturated 3 wt% NaCl	50 °C	4.0	24 h	Static stability
2	CO_2-saturated 3 wt% NaCl	50 °C	5.0	24 h	Static stability
3	CO_2-saturated 3 wt% NaCl	50 °C	5.5	24 h	Static stability

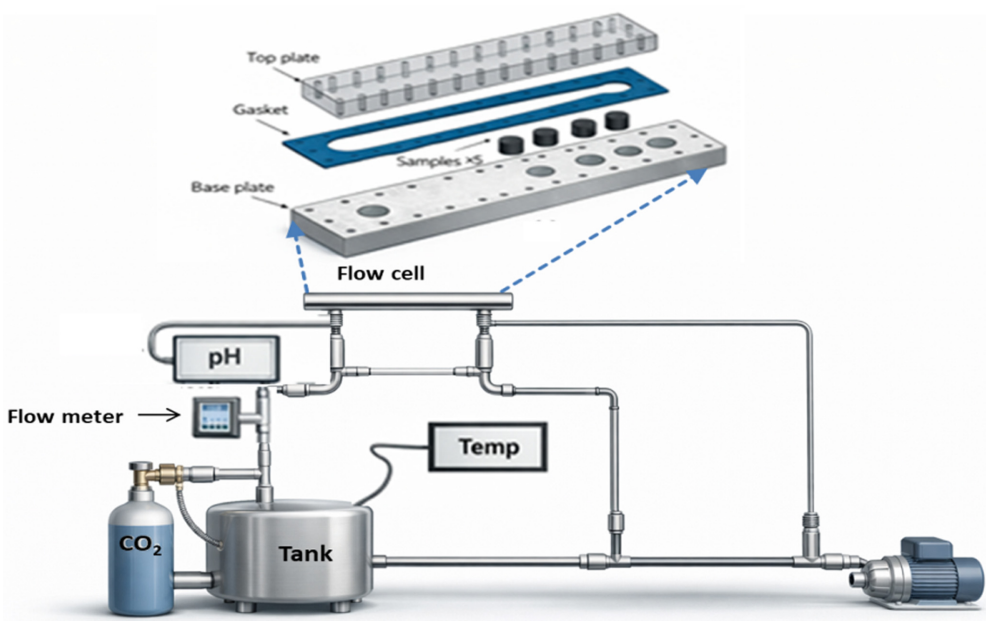

Fig. 2. Schematic diagram of the stepped-shear recirculating flow loop and test section geometry

containing 3 wt% NaCl, solution pH was adjusted to the target value (5.5) using sodium bicarbonate ($NaHCO_3$), and it was monitored throughout the experiment. The solution was purged overnight with CO_2 before testing, and continuous CO_2 bubbling was maintained throughout the experiments to prevent oxygen ingress. Temperature and pH were continuously monitored.

Pre-formed $FeCO_3$-coated specimens were removed from the autoclave, gently rinsed with distilled water and isopropyl alcohol, dried, and stored under vacuum prior to installation in the flow cell. Electrochemical measurements were performed using LPR under identical conditions to the static tests, with platinum wire counter electrodes positioned adjacent to each working electrode.

2.6 Surface Characterization

Following exposure, selected samples were allowed to air dry and then stored in a vacuum-deaerated jar to prevent oxidation and corrosion. Then, samples were examined using scanning electron microscopy (SEM) to assess surface morphology and film integrity. Energy-dispersive spectroscopy (EDS) was used to confirm film composition. Film thickness was determined from cross-sectional SEM images using multiple measurements at different locations along each cross-section, and values are reported as mean ± standard deviation.

3. Results

3.1 Formation and Growth of $FeCO_3$ Films under High-Pressure CO_2

Fig. 3 shows the corrosion behavior of X65 carbon steel exposed to CO_2-saturated aqueous conditions at 100 bar and 60 °C, over different immersion times. At the beginning of exposure, the corrosion rate was relatively high, but it decreased markedly within the first 24 h, with an approximately 25% reduction compared with the initial value. Over the same period, cumulative mass loss continued to increase.

After 48 h of exposure, the corrosion rate declined further and reached a low, nearly constant value, while cumulative mass loss approached a stable trend. The corrosion rate remained essentially unchanged up to 192 h, indicating that the steel surface had become covered by a protective corrosion product layer. The stable corrosion rate and mass-loss behavior suggest that this layer had reached a condition in which film growth and dissolution were balanced. Based on these results, 48 h was selected as the standard film-forming period for subsequent experiments.

Fig. 4 shows SEM surface and cross-sectional images of the corrosion products formed on X65 samples at different immersion times. After 6 hours of exposure (Fig.

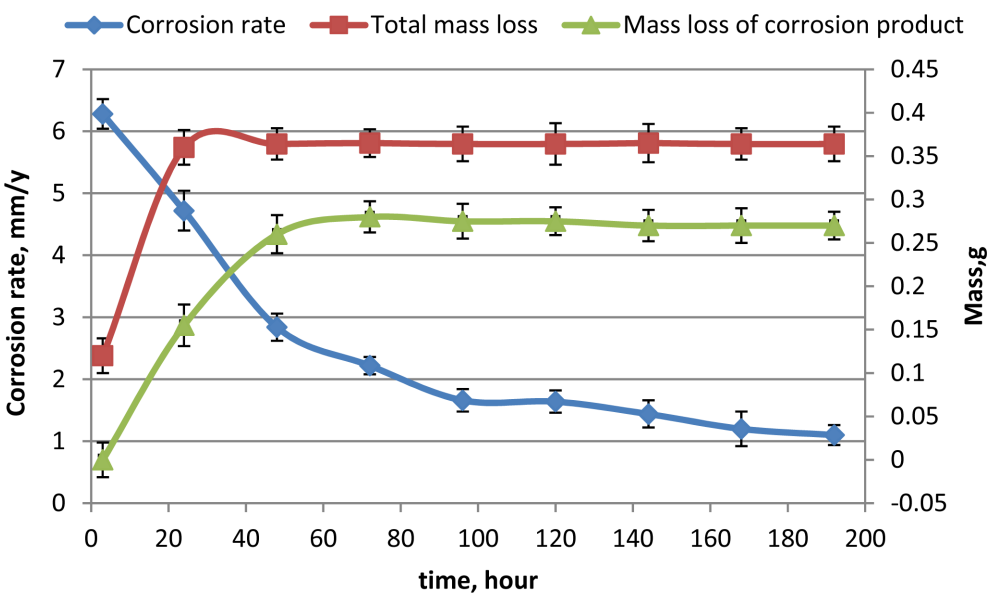

Fig. 3. Corrosion rate and cumulative mass loss of X65 carbon steel exposed to CO_2 at 100 bar and 60 °C as a function of immersion time. The stabilization of both curves indicates the formation of a dense protective $FeCO_3$ film

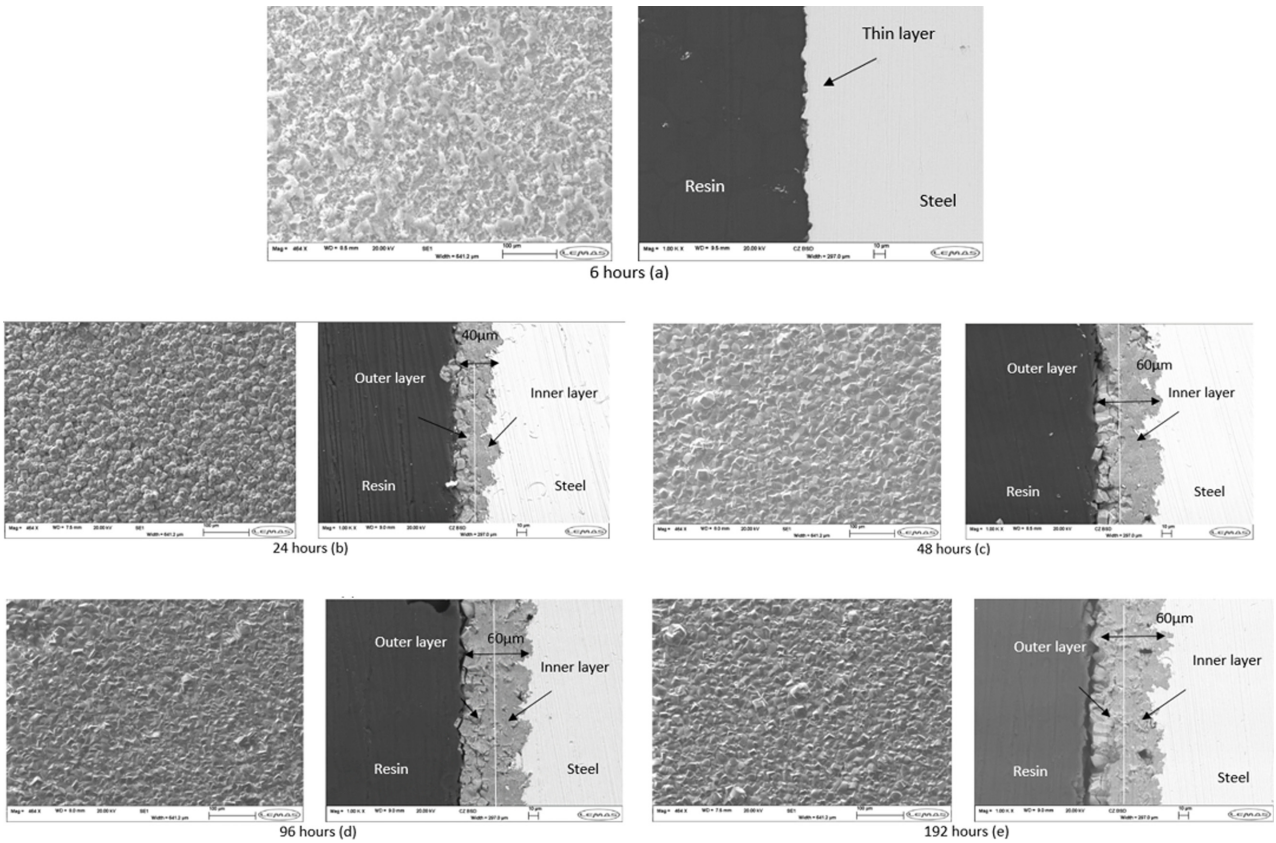

Fig. 4. SEM surface and cross-sectional images showing the evolution of corrosion product morphology and film thickness on X65 carbon steel after different immersion times at 60 °C and 100 bar CO_2. Scale bars indicate film thickness

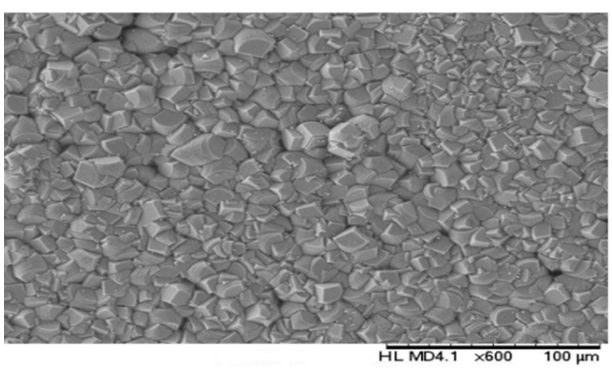

Fig. 5. High-magnification SEM image of the $FeCO_3$ film after 48 h immersion, showing densely packed prism-shaped crystals forming a compact protective layer

4a), sparse corrosion products were present on the surface, with large areas of bare steel still visible. The corresponding cross-section revealed only a very thin corrosion product layer. After 24 h (Fig. 4b), the surface was fully covered with prism-shaped iron carbonate crystals, and a continuous film with a thickness of approximately 40 µm was observed in the cross-section. The film structure consisted of an inner compact layer and an outer crystalline layer.

After 48 hours of exposure (Fig. 4c), the corrosion product film exhibited a dense, compact morphology across the entire surface, with an average thickness of approximately 60 µm. No further increase in film thickness or changes in microstructure were observed when the immersion time was increased to 96 and 192 hours (Fig. 4d and e), confirming that steady-state film growth had been achieved. High-magnification SEM image (Fig. 5) clearly showed packed prism-shaped $FeCO_3$ crystals forming a compact surface layer.

3.2 Static Stability of $FeCO_3$ Films as a Function of Solution pH

Under static aqueous CO_2 conditions at 50 °C for solution pH values of 4, 5, and 5.5, the stability of pre-formed $FeCO_3$ films was assessed. Fig. 6 illustrates how the corrosion rate of $FeCO_3$-coated X65 carbon steel changes over time.

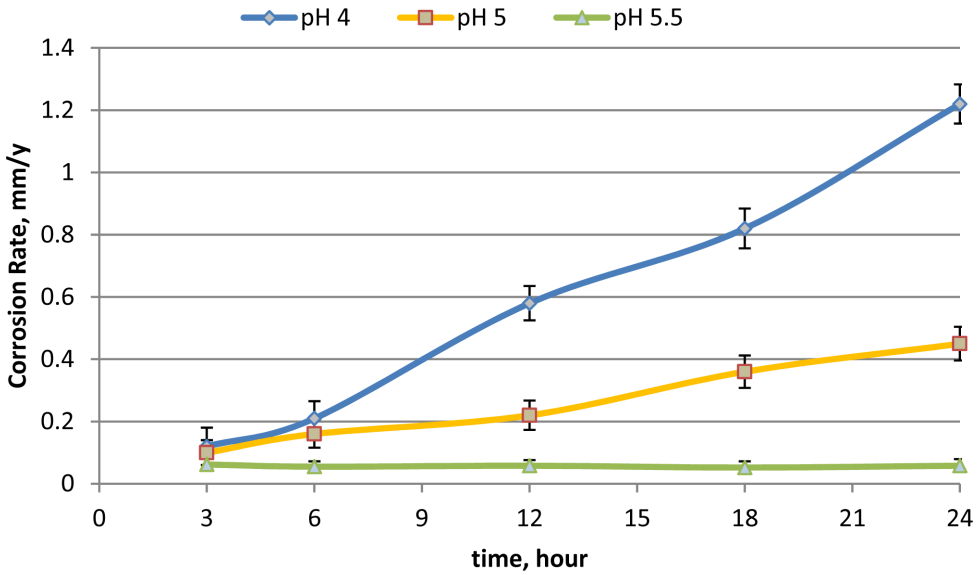

Fig. 6. Corrosion rates of the covered surface with protective films at different pHs & 50 °C for different solution pH values over 24 h exposure

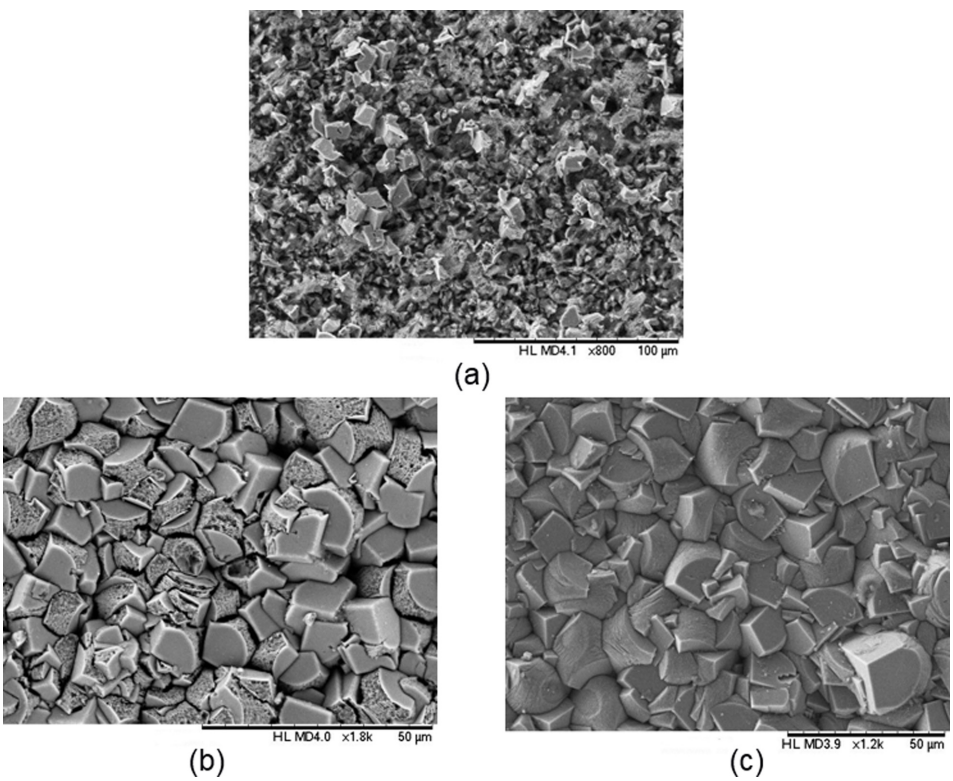

Fig. 7. SEM images of the protective films on the X65 carbon steel surface at 50 °C after 24 h exposure, (a) pH 4 showing severe film dissolution, (b) pH 5 showing partial degradation, and (c) pH 5.5 showing a continuous intact protective film

At pH 4, initial corrosion rates increased rapidly with exposure time, reaching approximately 0.12–0.15 mm/y during the first 3 h, and after 24 h, increased sharply, exceeding 1.2 mm/y. SEM surface topography image of the protective films after 24 h (Fig. 7) indicated severe damage to the $FeCO_3$ film, including crystal dissolution

and extensive exposure of the steel surface.

At pH 5, the corrosion rate of the samples remained relatively stable at approximately 0.1 mm/y for the first 6 h of exposure, after which it gradually increased. By the end of the 24 h test, corrosion rates reached approximately 0.45 mm/y, which is significantly lower than rates measured at pH 4. SEM observations of the surface after testing (Fig. 7b) showed that the $FeCO_3$ film largely remained intact but exhibited localized areas of degradation and increased surface porosity.

In contrast, at pH 5.5, corrosion rates remained stable and constant behavior throughout the 24 h test period, with approximately 0.06 mm/y. SEM examination after testing (Fig. 7c) confirmed the presence of a continuous and compact $FeCO_3$ film, where no visual signs of film removal were present.

3.3 Effect of Flowing Conditions on $FeCO_3$ Film Stability

The $FeCO_3$ film stability in flowing conditions was evaluated at the critical pH of 5.5 and a temperature of 50 °C, using wall shear stresses ranging between 10 and 655 Pa. Fig. 8 shows the corrosion rate curves exposed to different wall shear stresses as a function of time for $FeCO_3$-coated X65 carbon steel samples, where the dashed line indicates the transition boundary.

The results demonstrate progressive loss of protectiveness at high wall shear stress due to flow-enhanced dissolution and mass transfer effects rather than sudden mechanical detachment. At a wall shear stress of 655 Pa, the 10-fold jump in corrosion (0.4 to 4 mm/y) signifies total film removal. The linear increase suggests that once the barrier is breached, the underlying steel is fully exposed to the CO_2 environment. While at a wall shear stress of 300 Pa, still damaging, this stress level resulted in a 65% lower corrosion rate than the 655 Pa test. This indicates that the film might be thinned or porous rather than completely removed, or that the mechanical removal is occurring at a much slower rate.

When wall shear stresses were 65 Pa and 171 Pa, the corrosion rates did not show a significant increase, reaching approximately 0.8 mm/y and 1.0 mm/y after 24 hours, respectively. Although the shear stress of 65 Pa was 60% lower than that of 171 Pa, the corrosion rate was only 20% higher, indicating that the reduction in corrosion rate with decreasing wall shear stress was non-linear.

At 37 Pa of wall shear stress, a slight increase in the corrosion rate was observed, reaching about 0.61 mm/y at the end of testing. At lower wall shear stresses of 18 and 10 Pa, corrosion rates showed a low, stable behavior from the start to the end of the test. The relationship between wall shear stress and corrosion rate was non-

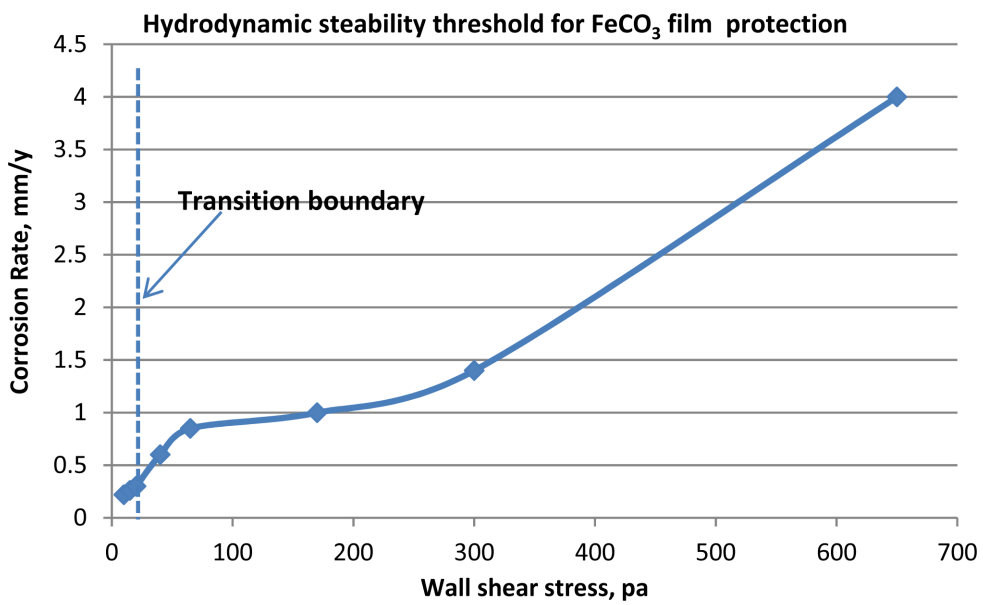

Fig. 8. Corrosion rate as a function of wall shear stress at pH 5.5 and 50 °C after 24 h exposure, showing0 a hydrodynamic stability threshold separating protective and non-protective regimes

linear. At low wall shear stress, the corrosion rate remained nearly constant because the $FeCO_3$ film retained its protective properties. At higher wall shear stress, the corrosion rate increased more rapidly as enhanced mass transfer promoted local film dissolution and loss of protection.

The combined influence of solution chemistry and hydrodynamic conditions on $FeCO_3$ film stability is summarized in the flow-chemistry regime map shown in Fig. 9. The diagram integrates the experimentally determined critical pH and wall shear stress thresholds from static and flowing tests. At pH values equal to or above 5.5 and wall shear stresses between approximately 10–18 Pa, the $FeCO_3$ films remained continuous and protective, indicating a stable regime. Outside this domain, progressive film degradation and increased corrosion rates were observed, indicating a transition to a non-protective regime. The regime boundary marks the experimentally observed transition between chemically stable and hydrodynamically unstable film behavior. The plotted markers indicate the tested conditions and demonstrate that film stability depends on the coupled effects of solution chemistry and flow intensity rather than on either parameter alone.

SEM surface and cross-sectional analysis (Fig. 10) revealed a clear correlation between wall shear stress and film degradation. At 655 Pa, SEM surface images showed extensive loss of the outer $FeCO_3$ layer, with large exposed regions of the steel surface, irregular cavities, and pronounced surface roughening. Cross-sectional observations confirmed severe thinning of the film (60 ±2 μm to less than 5 μm), indicating substantial loss of protectiveness under this condition.

At 300 and 171 Pa, SEM images showed partial film removal and discontinuous surface coverage, with localized defects and thinning zones distributed across the surface. These features suggest progressive degradation of the protective layer rather than complete film detachment.

At 65 and 37 Pa, much of the $FeCO_3$ film remained present, although localized degradation and partial thinning were visible. The persistence of crystalline film remnants indicates that degradation was limited under these conditions.

At 10 Pa, the SEM images showed a dense and continuous $FeCO_3$ layer with no obvious surface discontinuities or significant thinning, confirming that the film remained stable and protective under this condition (Fig. 10).

These findings indicate that under flowing conditions at pH 5.5 and 50 °C, the results indicate a transition region between 10 and 18 Pa, below which the film remained stable over 24 h and above which progressive degradation became detectable. The results in show three hydrodynamic regimes: a stable regime at low wall shear stress, specifically 10 Pa, where the $FeCO_3$ film remained

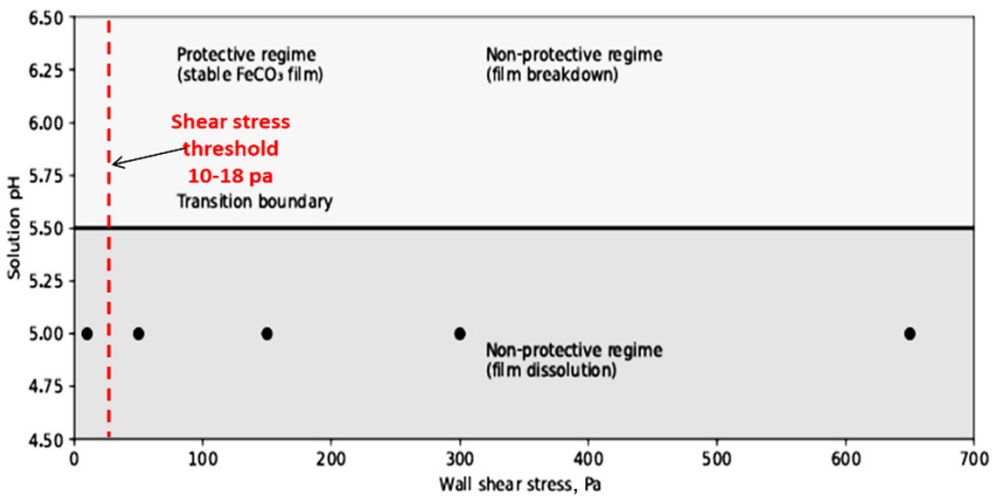

Fig. 9. Schematic flow–chemistry regime map illustrating $FeCO_3$ film stability as a function of wall shear stress and solution pH at 50 °C

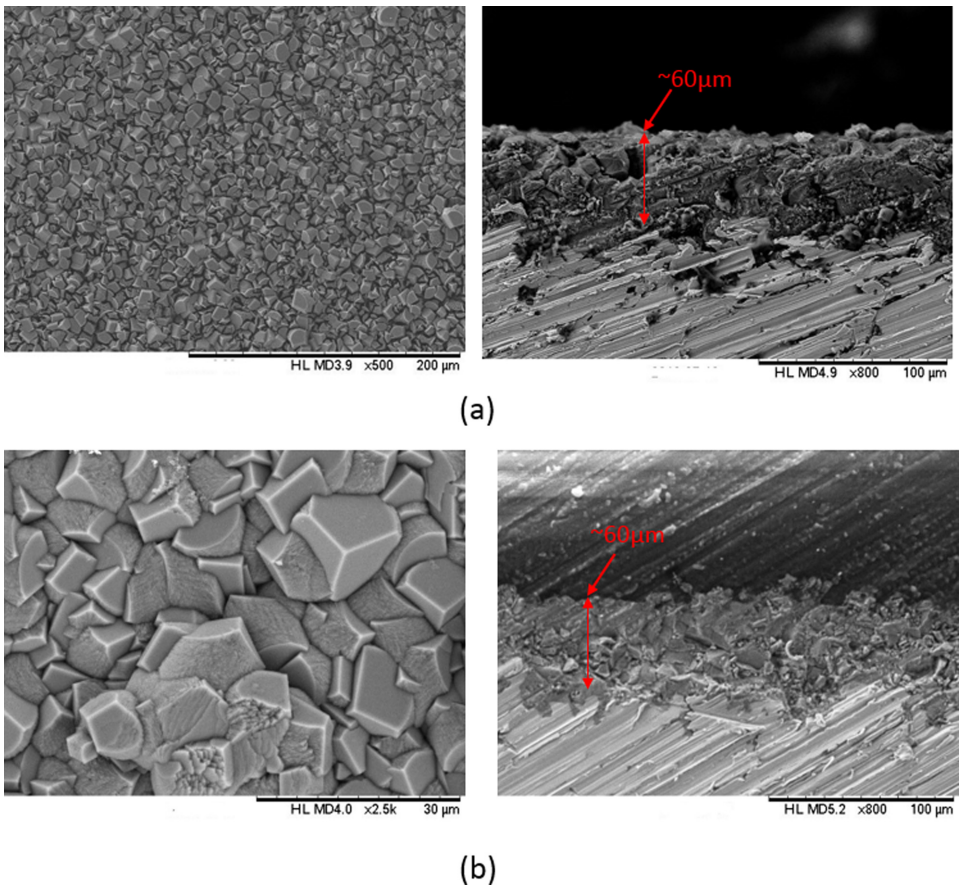

Fig. 10. SEM surface and cross-sectional of the protective films after 24 h exposure to 10 Pa wall shear stress, showing preservation of a dense and continuous protective layer

protective; a transition region between approximately 10 and 18 Pa, where early signs of film destabilization appeared; and a clearly non-protective regime at higher wall shear stress, where a marked increase in corrosion rate accompanied progressive film degradation.

3.4 Morphological Evolution of $FeCO_3$ Films under Increasing Shear Stress

The morphological evolution of $FeCO_3$ films formed on X65 carbon steel was examined after 24 h exposure to flowing conditions at 50 ºC and pH 5.5 over wall shear stresses ranging from 10 to 655 Pa.

$FeCO_3$ films on X65 carbon steel evolve from a dense, 100% surface-covering layer at low stress (10–18 Pa) to a highly fragmented, non-protective layer at high stress (655 Pa) due to flow-accelerated dissolution and mechanical removal. SEM surface and cross-sectional analyses quantify this, showing a progressive decline in film thickness and integrity as the hydrodynamic threshold is exceeded, with the film thickness decreasing from 60±2 µm before flow exposure to ~5 µm after 24 hours. Elemental mapping (Fig. 11) shows the distribution of elements in the cross-section view, with Fe, O, and C detected, confirming that the metal–film interface is a residual iron carbonate ($FeCO_3$).

At a wall shear stress of 300 Pa, SEM examination after exposure showed localized degradation of the $FeCO_3$ layer. Portions of the film were removed from some of the surface regions, resulting in discontinuities across the surface and the formation of irregular cavities and surface asperities. Cross-sectional analysis (Fig. 12) indicated that the residual film thickness was approximately 8 µm. Compared to the 655 Pa conditions, a larger portion of the film remained intact; however, the protective layer was no longer continuous across the surface.

In the 18 Pa to 37 Pa range, the first signs of stress appear. While the film remains continuous (covering the entire surface), it begins to thin slightly. This suggests that

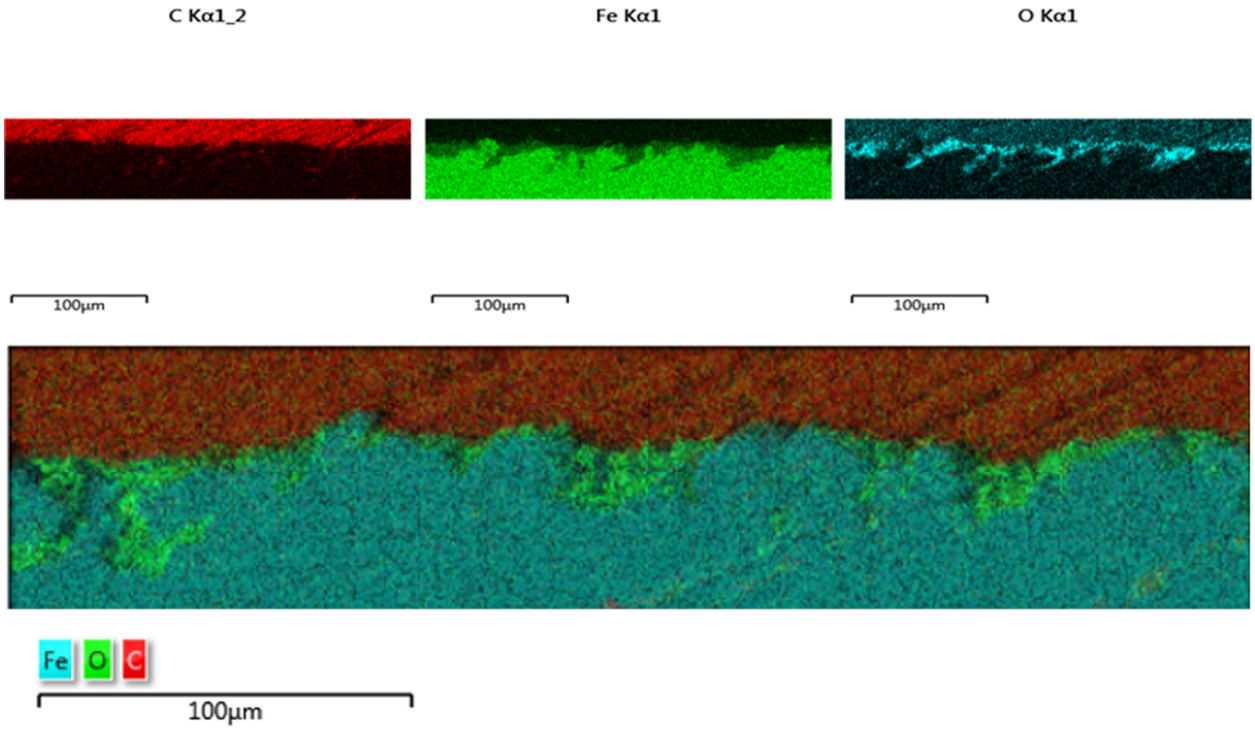

Fig. 11. Element mapping images of the iron carbonate films cross-section at 655 Pa after exposure, confirming the presence of residual iron carbonate at the metal–film interface

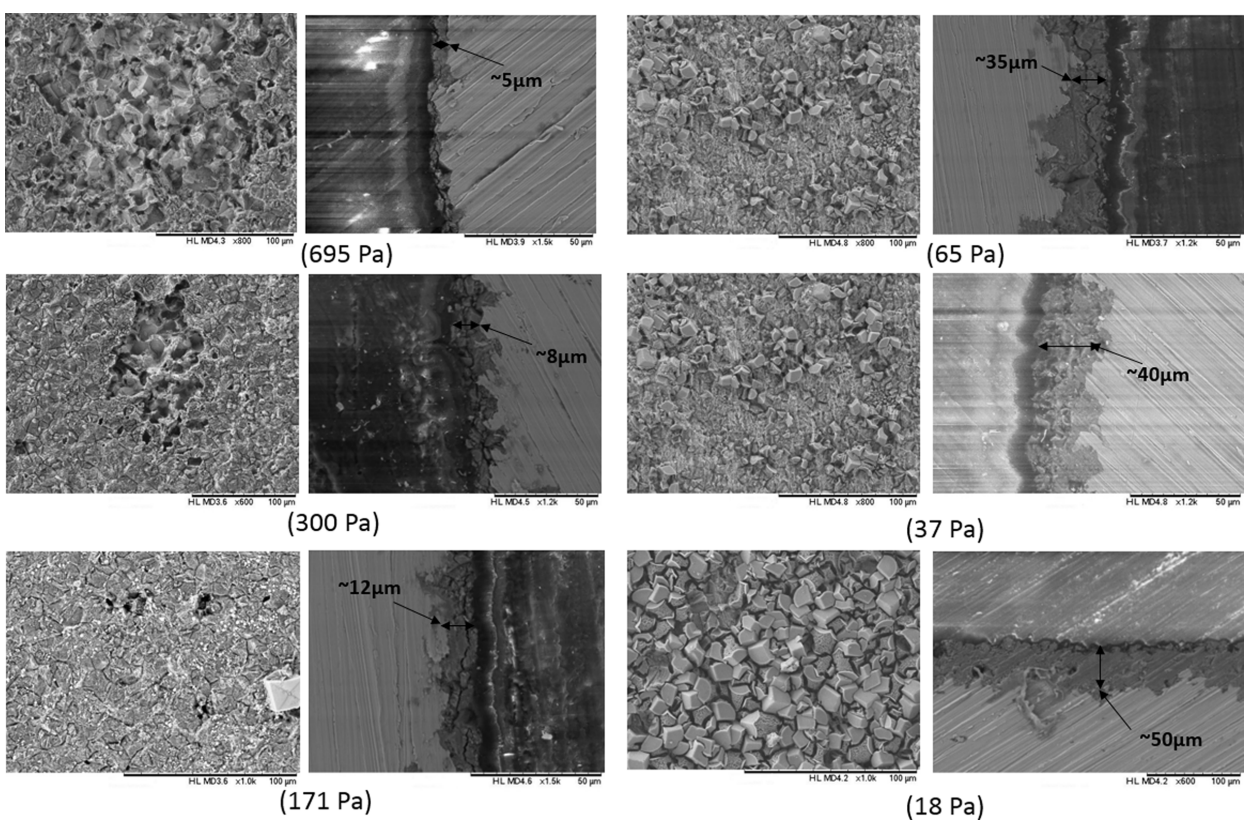

Fig. 12. SEM Surface and cross-section images of the protective films after 24 h exposure to flowing conditions with various wall shear stresses, illustrating progressive film thinning and removal with increasing hydrodynamic severity

the flow is not yet chunking off, but it is likely accelerating the dissolution of the outer crystal layers or causing very minor surface erosion.

Under intermediate wall shear stresses of 65 Pa to 171 Pa, this phase is the transition into the "non-protective" regime. The mechanical force is now strong enough to physically remove material. At 65 Pa, the film is residual, meaning it's being worn down. It has dropped to 35 μm (nearly half its original thickness). Whereas, at 171 Pa, damage becomes severe. The thickness was reduced to 12 μm, and localized defects (holes or pits) appeared. At this stage, the shield has failed, and the corrosive fluid can reach the steel through these gaps.

4. Discussion

4.1 Chemical Control of $FeCO_3$ Film Stability under Static Conditions

The static stability tests demonstrate that the protective properties of $FeCO_3$ films are strongly governed by solution chemistry, with solution pH as the primary controlling parameter at 50 ºC. Although dense, continuous $FeCO_3$ films formed during the initial high-pressure CO_2 exposure, their long-term stability in aqueous environments depended on the degree of solution saturation with respect to iron carbonate.

At lower pH values (pH 4 and 5), the aqueous phase is undersaturated with respect to $FeCO_3$, favouring chemical dissolution of the film even in the absence of hydrodynamic forcing.

In these conditions, the corrosion rate gradually increased over time reflects the slow loss of the film integrity as dissolution continues. The slower rise in corrosion rate observed at pH 5 compared to the fast rise at pH 4 is because $FeCO_3$ dissolves more slowly at higher pH, resulting in a delayed breakdown of the protective layer.

At pH 5.5 and 50 ºC, the solution becomes saturated with $FeCO_3$, which significantly reduces the thermodynamic driving force for dissolution. During the static exposure period, corrosion rates remained low and stable, and SEM analysis confirmed that the film stayed continuous and compact. This behavior shows that a chemically favorable environment can maintain film stability even when there is no flow. The identification of pH 5.5 as a critical threshold for $FeCO_3$ film stability in static environments aligns with previous studies on CO_2 corrosion of carbon steel [19,24], which have demonstrated that minor fluctuations in pH can significantly influence $FeCO_3$ solubility and film protective properties.

These findings confirm that the stability of $FeCO_3$ films in stagnant environments is governed by thermodynamic and kinetic parameters associated with solution chemistry; however, the results also show that chemical stability alone is insufficient to keep films from breaking down in flowing conditions, where mass-transfer processes become more dominant.

4.2 Flow-Enhanced Dissolution of $FeCO_3$ Films

The results indicate that in flowing environments, the stability of the $FeCO_3$ film is predominantly governed by hydrodynamic factors, even when the solution chemistry lies within the stability range established under static conditions. $FeCO_3$ films remained stable in stagnant environments at a pH of 5.5 and a temperature of 50 ºC; however, when flow was introduced, the films began to degrade once a critical wall shear stress was reached. This observation highlights the limitations of static corrosion tests for predicting film performance in real pipeline conditions.

SEM analysis indicated that increasing wall shear stress led to a progressive thinning and removal of the $FeCO_3$ layer rather than a sudden mechanical detachment. When the shear stress was high (≥ 300 Pa), the outer film layer was mostly lost, which made the film thickness go from 60±2 μm to only a few micrometres. Elemental mapping confirmed that the remaining interfacial layer consisted of iron carbonate, indicating that degradation proceeded through gradual removal of the outer crystalline layers rather than spallation of the entire film. This behavior is inconsistent with purely mechanically driven failure and instead points to a chemically controlled removal mechanism.

This interpretation is supported by the non-linear relationship between corrosion rate and wall shear stress. Corrosion rates increased rapidly at elevated shear stresses, whereas only minor changes were noted at shear stresses below approximately 10–18 Pa, where films remained intact. Such threshold behavior suggests that hydrodynamics do not directly remove $FeCO_3$ films through shear forces alone but enhance the kinetics of

chemical dissolution processes. Increased wall shear stress is expected to reduce the thickness of the hydrodynamic boundary layer, thereby enhancing mass transfer of dissolved species away from the film–solution interface. This promotes local undersaturation with respect to $FeCO_3$ at the interface, even when the bulk solution remains nominally saturated.

Surface morphology is also essential in the degradation process. SEM images showed that removing part of the film at intermediate shear stresses creates localized pits and gaps that increase the surface roughness. These characteristics can increase near-wall turbulence and improve local mass transfer. This promotes a positive feedback mechanism that accelerates film degradation over time. As the $FeCO_3$ film gets thinner, the remaining layer's ability to protect decreases, resulting in higher corrosion rates.

When the wall shear stress was below 37 Pa, portions of the $FeCO_3$ film stayed intact. Even after 24 hours of exposure, the residual thicknesses were still more than 30 μm. Under these environments, the enhancement of mass transfer does not seem to be sufficient to destabilize the film, and the rates of corrosion stay low and stable. There is a critical wall shear stress observed between about 10 and 18 Pa, which marks the threshold at which film behavior changes from stable to unstable under flow.

These results show that the degradation of $FeCO_3$ films in flowing conditions is governed by chemically driven dissolution processes that are greatly sped up by hydrodynamic mass transfer rather than by direct mechanical removal. This shows the need to consider how the chemistry of the solution and the flow of the mass transfer work together when evaluating the risk of corrosion and how well a protective film works in CO_2-containing carbon steel pipelines.

4.3 Implications for CO_2 Corrosion in Carbon Steel Pipelines

The results have direct implications for evaluating and mitigating CO_2 corrosion in carbon-steel pipelines. It demonstrates that the stability of protective $FeCO_3$ films cannot be assessed solely by solution chemistry, as films that exhibit chemical stability under static conditions may undergo considerable degradation in realistic flow environments.

Wall shear stress in operating pipelines often exceeds the critical threshold identified in this work. This is especially true in areas of high flow, diameter changes, bends, and flow restrictions. In these places, stable $FeCO_3$ films at a favorable pH can thin or be removed. As a result, corrosion rates rise. This shows the limits of predicting corrosion based solely on bulk water chemistry or static laboratory data.

The observed threshold in film stability indicates that corrosion risk in CO_2-carbon steel pipelines may vary along the flow path, even with uniform chemistry. Increasing local hydrodynamic wall shear stress can destabilize protective layers and create spots more prone to corrosion. This mechanism explains why extremely high local pipeline corrosion can appear despite the formation of $FeCO_3$ scale.

These results show how important it is to include hydrodynamic factors in corrosion risk assessments and plans for mitigation strategies. To preserve the film integrity during operation, it may be necessary to control the flow, modify the design to minimize high-shear areas, and select corrosion inhibitors. Also, identifying critical pH and shear stress thresholds provides valuable insights for developing and calibrating mechanistic CO_2 corrosion models that take into account both chemical and hydrodynamic effects.

Overall, this study shows that a coupled chemical-hydrodynamic framework is needed to assess the protective efficacy of $FeCO_3$ films in carbon-steel pipelines. This method is necessary to improve the reliability of corrosion predictions and ensure the long-term integrity of pipelines operating in CO_2-rich environments.

Although the present experiments were performed under single-phase aqueous flow, the results still offer mechanistic guidance for multiphase systems, where local shear and mass-transfer intensity can be even more variable. Direct extrapolation of the transition range reported here to multiphase flow is not appropriate, but the observed coupling between film stability and hydrodynamically enhanced mass transfer is expected to remain relevant.

Overall, this study shows that a coupled chemical-hydrodynamic framework is needed to assess the protective efficacy of $FeCO_3$ films in carbon-steel

pipelines. This method is necessary to improve the reliability of corrosion predictions and ensure the long-term integrity of pipelines operating in CO_2-rich environments.

5. Conclusions

Under the specific experimental conditions examined in this work, the results identify an experimentally observed hydrodynamic transition range separating stable and progressively degrading $FeCO_3$ film behavior. The main conclusions are as follows:

· Dense $FeCO_3$ films were formed during the autoclave stage and reached an approximately steady thickness after 48 h under the film formation conditions used in this work.

· Under static aqueous CO_2 conditions at 50 ºC, pH 5.5 provided the most stable environment for maintaining film integrity over the test period, whereas lower pH values promoted progressive dissolution.

· Under flowing conditions at pH 5.5 and 50 ºC, film degradation increased progressively with wall shear stress, showing that chemical stability under stagnant conditions did not guarantee stability under flow.

· The results indicate an experimentally observed hydrodynamic transition region between approximately 10 and 18 Pa, below which the film remained stable over 24 h and above which progressive thinning and loss of protectiveness became detectable.

· SEM and cross-sectional observations support a degradation mechanism dominated by flow-enhanced chemical dissolution and mass transfer rather than sudden mechanical detachment of the entire film.

· These findings should be interpreted within the limits of the present experimental conditions, namely X65 carbon steel, the $FeCO_3$ films formed in this study, and CO_2-saturated 3 wt% NaCl solution, 50 ºC challenge conditions, and single-phase flow in the present test geometry

Acknowledgments

The authors are grateful to the Petroleum and Gas Department and the University of Thi-Qar for their scientific support.

References

1. J. Chen, X. Wang, H. Ma, Z. Huo, Y. Wang, Experimental investigation on corrosion behavior of X80 pipeline steel under carbon dioxide aqueous conditions, ACS Omega, **7**, 6142 (2022). Doi: https://doi.org/10.1021/acsomega.1c06613
2. X. Wang, P. Yang, R. Li, G. Tong, J. Chen, Y. Wang, Investigation of supercritical CO_2 corrosion behavior of X80 carbon steel in pipelines: An in situ experimental and DFT study, The Journal of Supercritical Fluids, **213**, 106371 (2024). Doi: https://doi.org/10.1016/j.supflu.2024.106371
3. Z. Liu, Q. Gao, Research Progress on Major Influencing Factors of Corrosion Behavior of Pipeline Steel in Supercritical CO_2 Environment, Materials, **18**, 2424 (2025). Doi: https://doi.org/10.3390/ma18112424
4. J. Chen, X. Wang, H. Ma, Z. Huo, Y. Wang, Experimental Investigation on Corrosion Behavior of X80 Pipeline Steel under Carbon Dioxide Aqueous Conditions, ACS Omega, **7**, 6142 (2022). Doi: https://doi.org/10.1021/acsomega.1c06613
5. Y. Hua, S. Xu, Y. Wang, W. Taleb, J. Sun, L. Zhang, R. Barker, A. Neville, The formation of $FeCO_3$ and Fe_3O_4 on carbon steel and their protective capabilities against CO_2 corrosion at elevated temperature and pressure, Corrosion Science, **157**, 392 (2019). Doi: https://doi.org/10.1016/j.corsci.2019.06.016
6. R. Rizzo, S. Gupta, M. Rogowska, R. Ambat, Corrosion of carbon steel under CO_2 conditions: Effect of $CaCO_3$ precipitation on the stability of the $FeCO_3$ protective layer, Corrosion Science, **162**, 108214 (2020). Doi: https://doi.org/10.1016/j.corsci.2019.108214
7. S. A. Sadeek, C. Hale, F. E. Bedoya-Lora, K. S. Campbell, G. H. Kelsall, A. Hankin, Protectiveness and stability of iron carbonate films on carbon steel in mildly alkaline aqueous alkanolamine CO_2 environments, Corrosion Science, **227**, 111773 (2024). Doi: https://doi.org/10.1016/j.corsci.2023.111773
8. C. Wang, Improvement on the CO_2 corrosion prediction via considering the corrosion product performance. Corrosion Science, **217**, 111127 (2023). Doi: https://doi.org/10.1016/j.corsci.2023.111127
9. K. A. Mohammed, An Investigation of the Synergistic Influence of Surface Pipeline Temperature and Water condensation Rate on top-of-the-line corrosion of X65 steel in a CO_2 Vapour environment, South African Journal of Chemistry, **79**, 125 (2025). Doi: https://hdl.han-

dle.net/10520/ejc-chem-v79-n1-a13

10. P. Khunphakdee, B. Chalermsinsuwan, Review of flow accelerated corrosion mechanism, numerical analysis, and control measures, Chemical Engineering Research and Design, **197**, 519 (2023). Doi: https://doi.org/10.1016/j.cherd.2023.08.012
11. J. J. Arismendi Florez, J. V. Ferrari, Fluid flow effects on CO_2 corrosion: a review of applications of rotating cage methodology, Anti-Corrosion Methods and Materials, **66**, 507 (2019). Doi: https://doi.org/10.1108/ACMM-08-2018-1986
12. S. Nešić, Key issues related to modelling of internal corrosion of oil and gas pipelines–A review, Corrosion science, **49**, 4308 (2007). Doi: https://doi.org/10.1016/j.corsci.2007.06.006
13. M. Qin, S. Chen, N. Ye, Y. Chen, S. Zhang, K. Li, K. Liao, Study on the evolution mechanism and influencing factors of CO_2 corrosion product film under pipe flow, International Journal of Pressure Vessels and Piping, **216**, 105506 (2025). Doi: https://doi.org/10.1016/j.ijpvp.2025.105506
14. R. H. Hausler, and G. Schmitt, Hydrodynamic and flow effects on corrosion inhibition, in CORROSION 2004, Association for Materials Protection and Performance, C2004-04402 (2004). Doi: https://doi.org/10.5006/C2004-04402
15. Y. Liu, H. Jiang, T. Xu, Y. Li, CO_2 corrosion prediction on 20# steel under the influence of corrosion product film, Petroleum, **9**, 427 (2023). Doi: https://doi.org/10.1016/j.petlm.2021.07.003
16. Q. Li, W. Jia, K. Yang, W. Dong, and B. Liu, CO_2 Corrosion behavior of X70 steel under typical gas–liquid intermittent flow, Metals, **13**, 1239 (2023). Doi: https://doi.org/10.3390/met13071239
17. V. Ruzic, M. Veidt, and S. Nešić, Protective iron carbonate films—Part 1: Mechanical removal in single-phase aqueous flow, Corrosion, **62**, 419 (2006). Doi: https://doi.org/10.5006/1.3278279
18. R. K. Singh, S. B. Arya, and J. Nayak, Flow-Assisted Corrosion of API X70 Pipeline Steel in Simulated CO_2 Saturated Indian Oilfield Water: A Study on the Influence of Flow Velocity, Materials Chemistry and Physics, **349**, 131767 (2025). Doi: https://doi.org/10.1016/j.matchemphys.2025.131767
19. S. Ieamsupapong, B. Brown, M. Singer, S. Nesic, Effect of solution pH on corrosion product layer formation in a controlled water chemistry system, Association for Materials Protection and Performance, C2017-09160 (2017). Doi: https://doi.org/10.5006/C2017-09160
20. O. A. Nafday, and S. Nesic, Iron carbonate scale formation and CO_2 corrosion in the presence of acetic acid, Association for Materials Protection and Performance, C2005-05295 (2005). Doi: https://doi.org/10.5006/C2005-05295
21. J. Liu, P. Wan, Q. Zhang, G. He, X. Xing, G. Cui, CO_2-saturated flow-induced corrosion of pipe elbow via experiments and simulation, Anti-Corrosion Methods and Materials, **72**, 894 (2025). https://doi.org/10.1108/ACMM-08-2024-3082
22. F. E. Furcas, S. Mundra, F. Somaini, O. B. Isgor, U. M. Angst, Steel dissolution in carbonate environments, Corrosion Science, **253**, 112899 (2025). Doi: https://doi.org/10.1016/j.corsci.2025.112899
23. ASTM Gl-03, Standard practice for preparing, cleaning, and evaluation corrosion test specimens, ASTM international (2003).
24. R. Neerup, I. A. Løge, G. M. Kontogeorgis, K. Thomsen, P. L. Fosbøl, Measurements and modelling of $FeCO_3$ solubility in water relevant to corrosion and CO_2 mineralization, *Chemical Engineering Science*, **270**, 118549 (2023). Doi: https://doi.org/10.1016/j.ces.2023.118549